Synergistic effects of novel battery manufacturing processes for lead/acid batteries: Part II: Mechanistic studies

A. ROCHLIADI[1,2], R. DE MARCO[1,*] and A. LOWE[1]

[1]*Department of Applied Chemistry, Curtin University of Technology, GPO Box U 1987, Perth, Western Australia, 6845, Australia*
[2]*Department of Chemistry, Institut Teknologi Bandung, Jalan Ganesha 10 Bandung 40132, Indonesia*
(e-mail: achmad@itb.ac.id)
(*author for correspondence, e-mail: r.demarco@exchange.curtin.edu.au)

Abstract

The mechanistic aspects of the beneficial effects of different manufacturing processes on the performance of lead/acid batteries have been studied using electrochemical impedance spectroscopy (EIS), X-ray diffraction (XRD) and scanning electron microscopy (SEM). The implications of grid etching, active material compression and spiking of active material with conductive additives, along with various combinations of these processes, on the PAM and positive electrode corrosion layer have shown that a combination of compression and conductive additives reduces the $PbSO_4$ content of both the positive active material (PAM) and the grid corrosion layer, leading to an enhancement in battery performance. Furthermore, the impact of the most promising battery manufacturing process on the kinetics of electrochemical processes occurring in the LAB, as studied using EIS, has shown that the charge transfer resistance of control cells in the fully discharged state increases with cycling, while the treated cells behaved like a near-perfect capacitor, yielding a negligible charge transfer resistance. EIS has shown that the kinetics of lead/acid battery processes in additive spiked and compressed cells is accelerated with respect to control cells.

1. Introduction

Recent studies [1] have demonstrated that a combination of positive active material compression and conductive additives yields a 30% enhancement in the performance of lead/acid batteries, as compared to the additive effects of isolated battery manufacturing processes. This synergistic effect is the subject of the present paper, and the authors have employed EIS, XRD and SEM to understand the mechanism of performance enhancement.

SEM is a powerful method that can be used to reveal the microstructural features of the corrosion layer that forms at the grid/active material phase [2–8]. In SEM, the nature and thickness of the corrosion layers arising from the different treatments may be examined. It is generally assumed that the thickness of the corrosion layer and, in particular any underlayers of PbO and/or $PbSO_4$, is related to poor performance. Several authors have reported ways to reduce the effects of the corrosion layer using different grid alloys and/or small additions of tin, aluminium, silver and cadmium in the alloys [9–13]. The corrosion underlayer of PbO could also be removed by etching the grid with sodium hydroxide prior to the pasting of plates; this step removes the basic lead carbonate phase that induces the formation of insulating PbO in the grid/active material layer [2].

XRD may be used to reveal the different lead phases in plates [3, 14–17]. Electrolyte stratification along with a diminution in the agglomeration of spheres, causes a reduction in the efficiency of lead/acid batteries, and are clearly related to a short term loss in performance [3, 18–20]. This process gives rise to $PbSO_4$, which can be analysed using XRD. Numerous authors [3, 20–27] have demonstrated that sulfation is one of the significant factors that causes a diminution in the conductivity of plates leading to premature capacity loss (PCL).

EIS is a powerful technique that provides important information about the electrical properties of the dynamically changing electrode–electrolyte interface, and has been used by several authors to investigate kinetic factors responsible for improvements in battery cycle-life [28–31]. The state of health (SOH) of the positive plate can be determined by evaluating the values of charge-transfer resistance, ion diffusion resistance, resistance of the grid–PAM interface, and ohmic resistance of the electrode, as revealed by EIS measurements [31].

2. Experimental details

2.1. *XRD sampling and analysis*

Samples from three positions (top, centre and bottom in Figure 1) of selected cycled plates were taken and ground together using a mortar and pestle. Previous experience has shown that the $PbSO_4$ content at the top of plates is negligible, moderate at the middle, and high at the bottom. This trend is highly reproducible; therefore a global average for each plate, representative of the bulk $PbSO_4$ content of plates, may be obtained by averaging the data for the three locations.

Samples were placed in a XRD sample holder. XRD measurements were performed using a Kristalloflex Siemens D500 diffractometer fitted with a CuK_α X-ray tube that operated at an accelerating voltage of 20 kV using a beam current of 30 mA. Measurement angles ranged from 5 to 100° with a step size of 0.4° and a speed of 2.4°/min.

2.2. *SEM sampling and analysis*

Cycled positive plates were cut and embedded in epoxy, which were used to produce polished cross-sections for examination by SEM. The samples were polished successively using 500, 1000 and 1200 grit emery papers using a paraffin lubricant and a Struers Dap-V polisher at a rotation speed of 300 rpm. After grinding, samples were polished on Struers DP-mol and then Struers DP-Nap cloths using diamond P sprays (3 and 1 μm) and Struers DP-red lubricant at a rotation speed of 300 rpm.

The polished epoxy-mounted samples were examined by SEM using a Philips XL30 electron microscope operated at an accelerating voltage of 20 kV, a spot size setting of 3, and a beam current of 60 pA.

2.3. *EIS studies*

EIS studies were performed by using a Solartron SI 1287 as the electrochemical interface, and the Solartron SI 1260 as t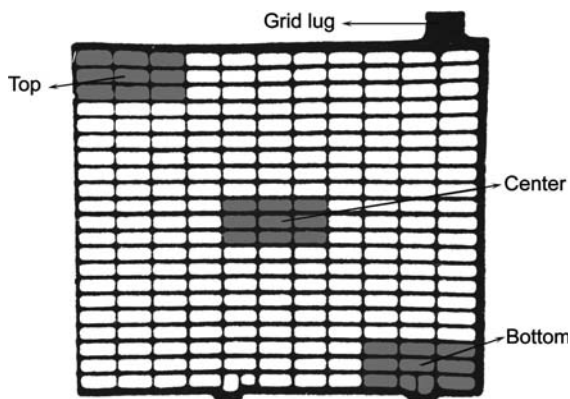he impedance/gain-phase analyser. Negative plates were used as the counter electrode, and the positive plate was the working electrode. This setting is consistent with the measurement technique applied by other researchers [29, 32, 33]. A separate reference electrode is placed between the positive and negative plates. In this study utilizing compressed cells, a platinum pseudo-reference was used for this purpose (Figure 2). With this assembly, the working and counter electrodes set up a net current while two separate reference electrodes (sense/positive plate and REF/platinum pseudo-reference) are placed to measure the potential difference between the two points where the impedance is to be measured. By using separate cables for current and potential sensing, potential drops in the cabling is eliminated from the measurement.

EIS measurements were recorded at four stages of the battery production and testing: (a) before formation, (b) after formation, (c) at full charge, and (d) at full discharge (Table 1).

The EIS control refers to whether the potentiostat controls the voltage or the current. Voltage control is used when high impedance is expected and current control is used for low impedances. The amplitude refers to the magnitude of the perturbation. The bias reflects the d.c. value of the perturbation and the bias also holds during intervals between measurements. It is used to maintain a trickle charge on the battery at full charge, so that it remains at full charge during EIS measurements.

3. Results and discussion

The authors' previous work [1] demonstrated that a melding of novel battery manufacturing processes (grid cleaning, positive active material compression and conductive additives to the positive paste) led to
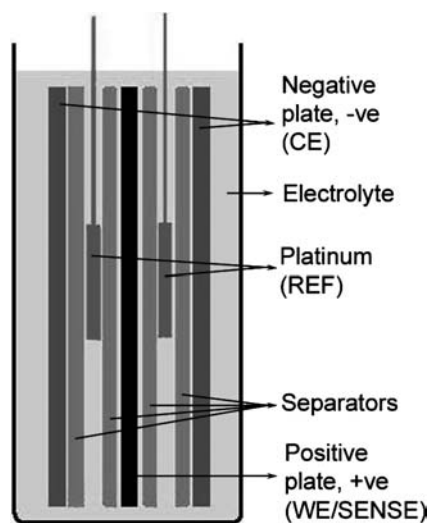

Fig. 1. Sampling scheme for the XRD phase analysis of failed LABs. Samples were collected from the top, centre and bottom (as shown).

Fig. 2. Schematic diagram of the electrochemical cell used to conduct EIS measurements on LABs. The negative plate was employed as the counter electrode (CE), while a platinum pseudo-reference electrode (REF) was employed so as to withstand the application of compressive loads, and the positive plate was made the working electrode (WE).

Table 1. EIS experimental parameters

Battery condition	EIS control	Amplitude	Bias	Frequency range
Unformed	voltage	10 mV	none	10 kHz
Formed	current	200 mA	none	10 kHz to 10 mHz
Fully charged	current	200 mA	10 mA	10 kHz to 10 mHz
Fully discharged	current	200 mA	none	10 kHz to 10 mHz

synergistic effects with regard to the cycling performance of lead/acid batteries. It has been found that a combination of positive active material compression and grid cleaning approximately doubles the durability of batteries and is consistent with the additive effects of the individual treatments, while a combination of positive active material compression and conductive additives yields an approximate 30% boost in performance compared to the additive effects of the isolated treatments.

The average phase compositions for each type of plate at the bottom, middle, and top of the plate are presented in Figure 3(a)–(c), respectively. The XRD data clearly show there is a relationship between the content of $PbSO_4$ and PbO_2 in plates, and the performance of cells. From the cycling results, the additive spiked + compressed plates achieved the best performance amongst all cells, and XRD revealed that this treatment reduced the $PbSO_4$ content at the bottom of the plate from 43.05% (control) to 15.61% (additive spiked + compressed), while increasing the PbO_2 content of plates from 56.23% to 84.39%, while other treatments do not have such a dramatic effect on the phase composition of plates. In the middle position, the corresponding difference in $PbSO_4$ content is 32.50% (control) to 11.30% (additive spiked + compressed), and there is an increase of the PbO_2 content from 67.50% (control) to 88.71% (additive spiked + compressed). No significant change in phase composition was noted at the top of the plate.

Clearly, tin oxide acts as a conducting bridge between particles in the positive active mass, while compression ensures an agglomeration-of-spheres (AOS) in the positive active mass, and these factors conspire to produce a synergistic effect, minimizing plate sulfation as a function of cycling.

The XRD phase composition data also revealed there is stratification of the sulfuric acid electrolyte in cells as a function of cycling. Significantly, a combination of compression and spiking with conductive additive reduces stratification of the electrolyte, as it can be seen that the percentages of the $PbSO_4$ at the top–centre–bottom of the control cells are 5.05%, 32.50% and 43.05%, respectively, while the additive-spiking and compression treatment gave a corresponding variation of 2.32%, 11.30% and 15.61%, respectively.

The SEM backscattered electron micrographs of cycled positive plates are presented in Figure 4(b)–(d) for single treatments, along with Figure 5(a)–(d) for combination treatments, respectively. The brightness of

the backscattered electron image corresponds to a compositional variation in the sample, for example, phases rich in heavy elements (e.g., Pb metal) are registered as bright spots, while phases low in heavy elements (e.g., PbO_2) give rise to dark spots. The intermediate layer of brightness at the grid/corrosion layer interface is attributable to an insulating PbO and/
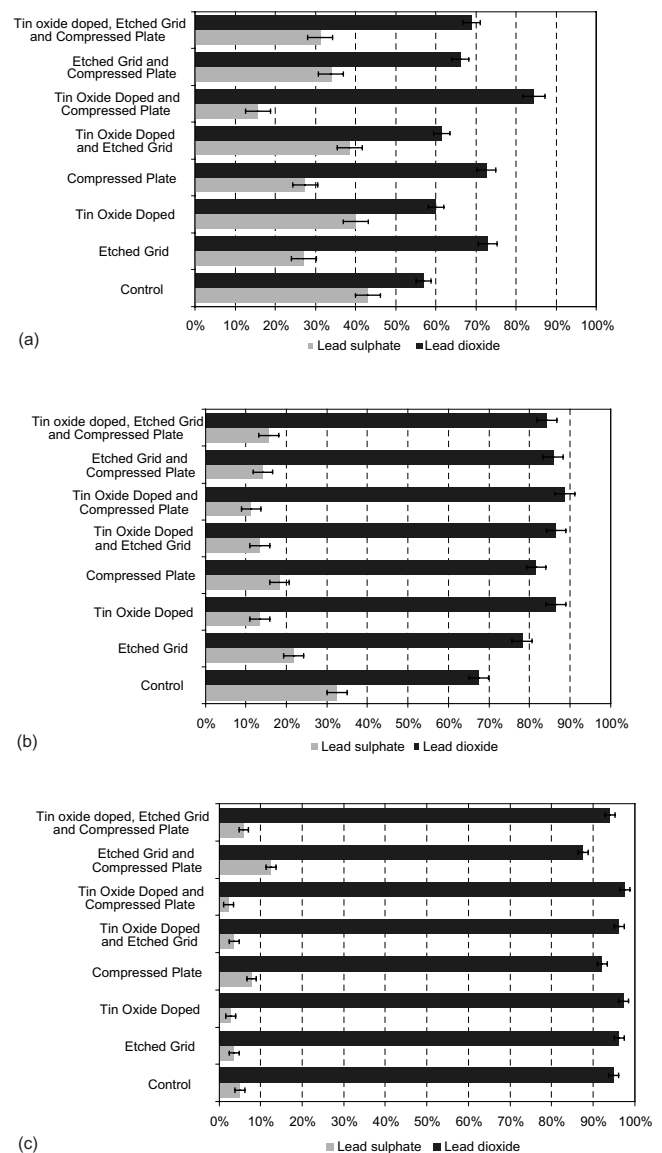

Fig. 3. Average XRD phase composition data at the following positions of failed LAB positive plates: (a) bottom, (b) centre and (c) top. At least six cells were analysed to provide this phase composition data.
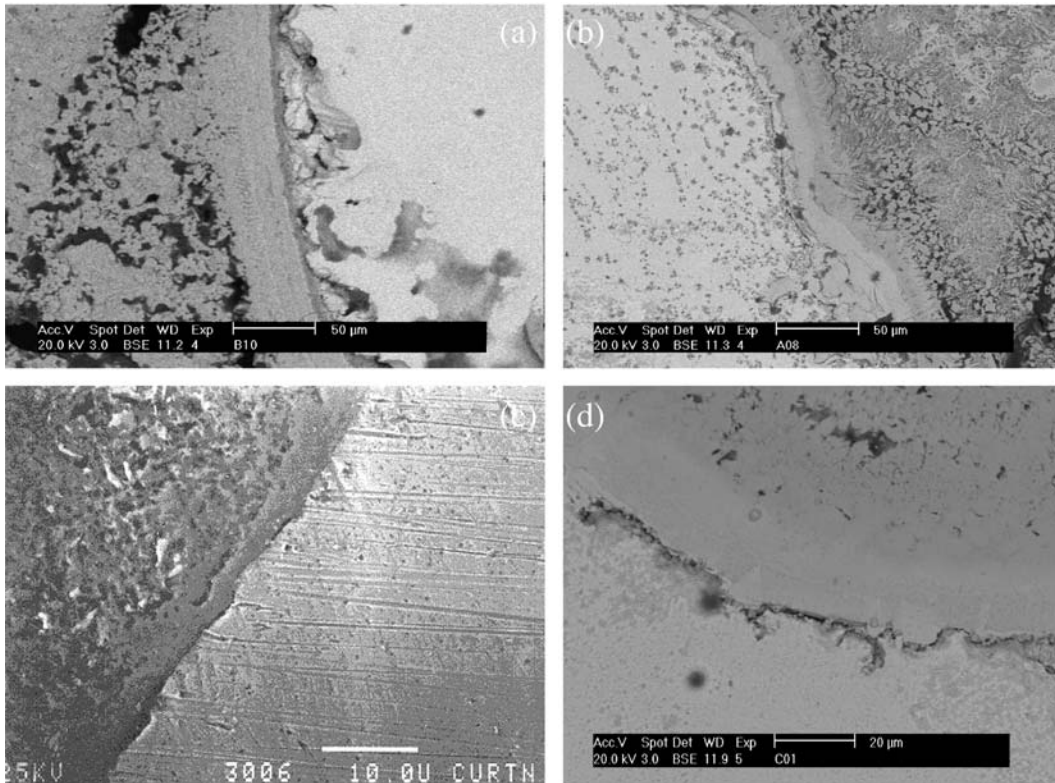
Fig. 4. SEM backscattered electron micrographs of polished cross sections of LAB positive plates subjected to single battery treatments: (a) control or untreated; (b) additive spiking of the PAM; (c) sodium hydroxide etching of the grid; (d) compression of the PAM.
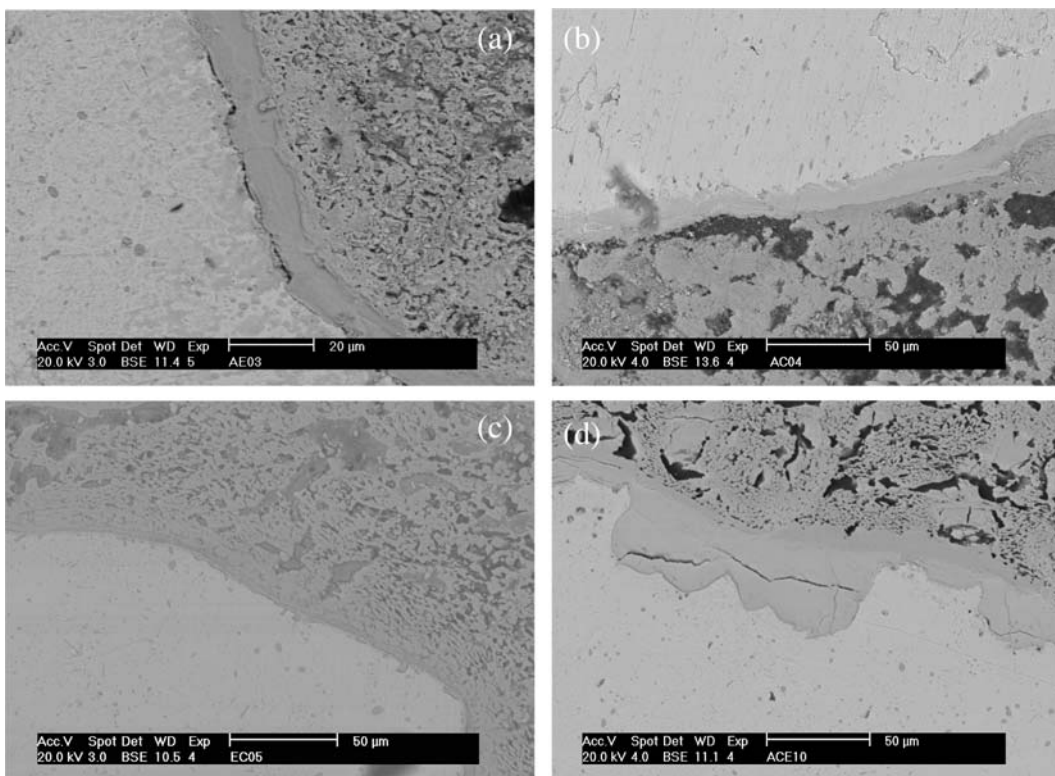

Fig. 5. SEM backscattered electron micrographs of polished cross sections of LAB positive plates subjected to combinations of battery treatments: (a) additive spiking of the PAM and sodium hydroxide etching of grids; (b) additive spiking and compression of the PAM; (c) sodium hydroxide etching of the grid and compression of the PAM; (d) additive spiking and compression of the PAM, along with sodium hydroxide etching of the grid.
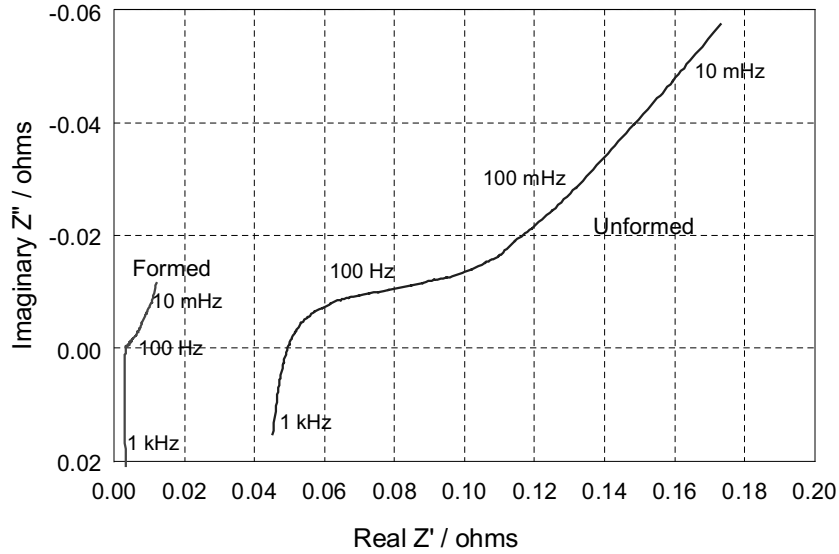
Fig. 6. EIS complex-plane impedance plots for an unformed and formed additive spiked and compressed LAB.

or $PbSO_4$ layer, which blocks charge transfer to the grid, and degrades the performance of the battery.

The SEM backscattered electron micrograph for the polished cross section of a control positive plate (Figure 4(a)) revealed a corrosion layer that is approximately 50 μm thick, and possesses a compositionally disparate underlayer. It can be seen that the different treatments alter the thickness of the corrosion layer, and the compositionally different underlayer, which is due presumably to PbO and/or $PbSO_4$. It is highly possible that this layer is not purely PbO, but instead a layer of PbO_n ($1 < n < 2$). Nevertheless, the aforesaid underlayer was removed/reduced by compression, grid etching and grid etching + compression treatments. It can also be seen that the PbO and/or $PbSO_4$ underlayer is indiscernible for the combination of all treatments, and this will undoubtedly have some implications for battery

performance. Although superior battery performance and synergistic effects were noted for a combination of active material spiking and plate compression [1], the aforesaid SEM evidence indicates that grid corrosion does not play a major role in the performance of lead/acid batteries.

Figure 6 presents EIS complex-plane impedance plots for the additive-spiked and compressed cell before and after formation, noting that all other cells displayed very similar behaviour and are therefore not reported herein. It is seen that the overall ohmic resistance of the electrode was reduced after plate formation, and is due to the conversion of nonconducting $3PbO \cdot PbSO_4$ to PbO_2 and Pb in the PAM and negative active material (NAM) during the formation process.

Figures 7 and 8 present EIS complex-plane impedance plots for the control along with compressed + additive
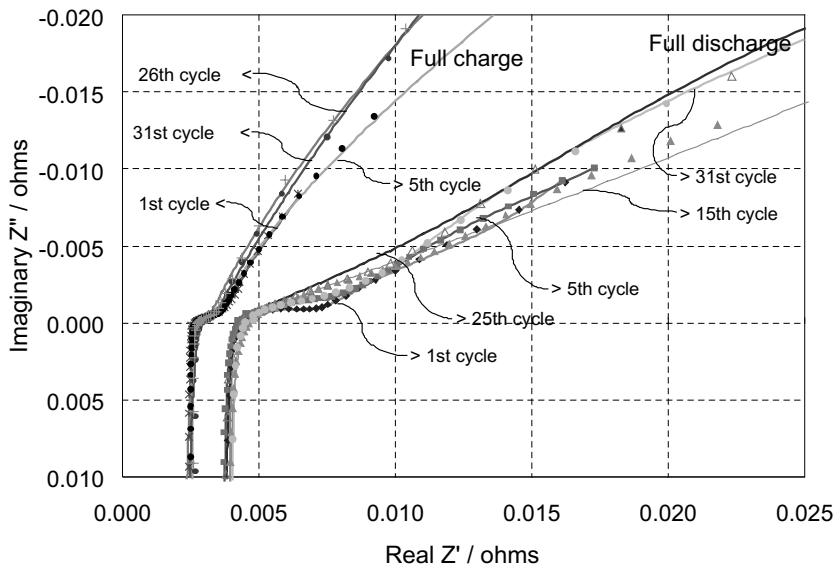

Fig. 7. EIS complex-plane impedance plots for a control LAB in the fully charged and discharged states as a function of charge/discharge cycling.
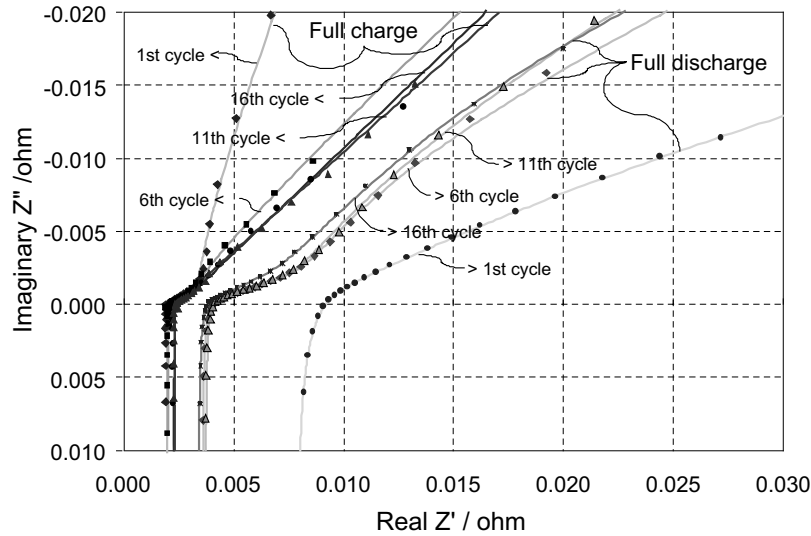
Fig. 8. EIS complex-plane impedance plots for an additive-spiked and compressed LAB in the fully charged and discharged states as a function of charge/discharge cycling.

spiked cells at different stages of cycling in the fully charged and discharged states. The equivalent electrical circuits best describing the EIS data are presented in Figure 9(a) and (b), and represent a slight modification of the circuit proposed by Pavlov [31]. For the data reported in this study, the inductance element (L1) was added to Pavlov's original circuit. R1 gives the total ohmic resistance of the electrode (i.e., the impedance of the PAM), the resistance of the thin layer connecting the PAM and the corrosion layer (CL + AMCL), and the resistance of the electrolyte, L1 is the inductance caused by the metallic connection between the poles and electrodes of the battery, CPE1 is a constant phase element representing the dielectric properties of the reaction layers, which is equivalent to an electrical capacitance, CPE2 is a constant phase element representing the diffusion processes for H^+ and SO_4^{2-} ion in the reaction layer, and R2 is the charge transfer resistance in the reaction layer, representing the electrochemical reaction process occurring at the interface and within the pores of the PAM and CL + AMCL. During discharge, the electrochemical reaction shifted from the bulk of the PAM to the CL + AMCL and necessitated the addition of new elements, R3 and CPE3. Note, R3 is the ohmic resistance of this CL + AMCL, and CPE3 is a con-

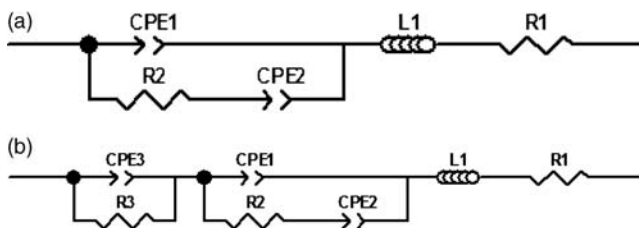stant-phase element representing the dielectric properties of the CL + AMCL layer [31].

A quantitative analysis of the experimental impedance data was performed using the nonlinear least squares minimization method developed by Boukamp [34]. The values of the electrical elements are summarized in Tables 2–5.

It is evident that the overall ohmic resistances, R_1, for both the control and treated LABs in the fully charged state are low compared to the fully discharged state. This is due the fact that fully discharged LABs comprise a higher content of $PbSO_4$, and the electrolyte concentration is at a minimum. In the fully charged state, the treated LAB has a slightly lower overall resistance, R_1, compared to the control LAB, indicating that the $PbSO_4$ content of the control LAB is marginally higher that of the treated cell.

There is no systematic pattern for the series inductance of the tested systems. This is due to the fact that the inductance, L, is caused by the metallic connection between the plate and the electrode, and these are no physical changes in this parameter during charge/discharge.

For the control cell, the charge transfer resistance, R_2 (Table 4), and CL + AMCL resistance, $R3$ (Table 4), is gradually increasing as a function of cycling in the fully discharged state. Conversely, the charge transfer resistance, R_2, of the fully discharge additive-spiked + compressed LAB is negligible throughout cycling (Table 5), which is symbolic of this element being a near perfect capacitor. Furthermore, the CL + AMCL resistance, R_3, in the fully discharged state of the treated cell displays a gradual decline as a function of cycling, which is symbolic of amelioration of the grid corrosion mode of PCL in the treated cell.

In summary, the AOS and conductive bridges formed between PAM particles as a result of a combination of

Fig. 9. EIS equivalent circuit models for (a) charged LABs and (b) discharged LABs.

Table 2. Equivalent circuit parameters for a charged control LAB

Cycle	R_1 /mΩ	L_1 /nH	CPE_1 /S	n_1	R_2 /mΩ	CPE_2 /S	n_2
1	2.4929	743.40	246.82	0.5724	1.9281	780.81	0.90
5	2.5428	695.78	324.22	0.5306	1.9607	1331.40	0.97
26	2.6395	577.53	327.78	0.6162	1.7848	779.40	1.00
31	2.7009	609.94	298.78	0.6181	1.6440	871.69	0.97

Table 3. Equivalent circuit parameters for a charged treated LAB

Cycle	R_1 /mΩ	L_1 /nH	CPE_1 /S	n_1	R_2 /mΩ	CPE_2 /S	n_2
1	1.9768	265.81	328.66	0.7177	2.5284	1107.60	1.00
6	1.9825	560.87	352.10	0.5366	1.4238	735.63	0.79
11	2.2152	430.84	368.01	0.5546	2.0197	394.62	0.74
16	2.2547	410.01	49.80	0.6609	0.3003	609.75	0.60

Table 4. Equivalent circuit parameters for a discharged control LAB

Cycle	R_1 /mΩ	L_1 /nH	CPE_1 /S	n_1	R_2 /mΩ	CPE_2 /S	n_2	CPE_3 /S	n_3	R_3 /mΩ
1	3.81	493.01	56.48	0.48	4.14	2261.90	0.68	2138.60	0.78	4.51
5	3.52	736.47	64.06	0.42	7.70	747.17	0.76	1054.50	0.89	6.52
15	3.42	744.96	64.84	0.34	57.96	49.99	0.74	558.04	1.00	7.42
25	3.55	633.20	71.31	0.39	90.51	12.60	1.00	637.63	0.97	10.78

Table 5. Equivalent circuit parameters for a discharged treated LAB

Cycle	R_1 /mΩ	L_1 /nH	CPE_1 /S	n_1	R_2 /mΩ	CPE_2 /S	n_2	CPE_3 /S	n_3	R_3 /mΩ
1	7.56	666.53	0.82	0.85	0.91	496.43	0.65	47.91	0.41	74.56
6	3.24	512.24	1431.50	0.96	0.00	93.57	0.30	181.31	0.27	21.39
11	3.53	502.81	421	0.78	4.79×10^{-16}	274	0.22	100	0.39	6.00
16	3.24	512.24	1430	0.96	3.94×10^{-16}	93.6	0.30	181	0.27	21.39

conductive additive spiking and compression of the active material enhances significantly the kinetics of the electrochemical process in the positive electrode of the LAB, as evidenced by the formation of a near-perfect capacitor with a negligible impedance for the charge transfer process. Also, the use of conductive additive spiking and compression of the PAM minimizes the CL + AMCL impedance of the positive electrode, obviating the grid corrosion mode of PCL.

4. Conclusions

All the treatments reported in this study enhance the performance of LABs. The most significant improvement was achieved via synergistic effects for conductive additives and plate compression, raising the performance of LABs by approximately 100%.

XRD phase analysis showed that conductive additives and plate compression reduced the amount of non conductive $PbSO_4$ in the positive active material on every position of the plate (top, centre, bottom), while in other treatments, plate sulfation is problematic. It is suggested that these factors are partly responsible for the synergism occurring in these systems.

EIS studies have demonstrated that kinetic effects are controlling the behaviour of LAB cells. It seems that the overall ohmic resistance of control cells is increasing slightly as a function of charge/discharge cycling. The overall ohmic resistance for treated LABs, based on conductive additives and compression, was found to be lower compared to the control cells.

Furthermore, the EIS results demonstrated that the use of compression and conductive additives within the PAM facilitated significantly the kinetics of the charge transfer process in the LAB, and this treatment also minimized the impact of grid corrosion on PCL.

The results of this study demonstrate unequivocally that the substantial boost in performance of LABs noted with conductive additives and compression is

attributable to the positive effects of the AOS and conductive bridges within the PAM on the kinetics and physicochemistry of the LAB. This is not surprising given that the single most important factor implicated in PCL of LABs is a loss in AOS as a consequence of the disintegration of the particle network in the PAM.

Acknowledgements

References

1. A. Rochliadi and R. De Marco, *J. Appl. Electrochem.* **32** (2002) 1039.
2. R. De Marco, A. Rochliadi and J. Jones, *J. Appl. Electrochem.* **31** (2001) 953.
3. R. De Marco and J. Jones, *J. Appl. Electrochem.* **30** (2000) 77.
4. Q. Dengke, *J. Power Sources* **78** (1999) 88.
5. E. Meissner, *J. Power Sources* **78** (1999) 99.
6. B. Culpin, A.F. Hollenkamp and D.J. Rand, *J. Power Sources* **38** (1992) 63.
7. N.E. Bagshaw, *J. Power Sources* **67** (1997) 105.
8. I. Petersson and E. Ahlberg, *J. Power Sources* **91** (2000) 143.
9. S. Zhong, H-K. Liu, S-X. Dou and M. Skyllas-Kazacos, *J. Power Sources* **59** (1996) 123.
10. S. Fouache, A. Chabrol, G. Fossati, M. Bassini, M.J. Saiz and L. Atkins, *J. Power Sources* **78** (1999) 12.
11. J.L. Caillerie and L. Albert, *J. Power Sources* **67** (1997) 279.
12. M.K. Dimitrov and D. Pavlov, *J. Power Sources* **93** (2001) 234.
13. E. Rocca and J. Steinmetz, *Electrochim. Acta* **44** (1999) 4611.
14. N. Cui and J.L. Luo, *Electrochim. Acta* **45** (2000) 3973.
15. R. De Marco and J. Liesegang, *Appl. Surf. Sci.* **84** (1995) 237.
16. R.J. Hill, A.M. Foxworthy and R.J. White, *J. Power Sources* **32** (1990) 315.
17. I. Petersson and E. Ahlberg, *J. Power Sources* **91** (2000) 137.
18. J. Apâteanu, A.F. Hollenkamp and M.J. Koop, *J. Power Sources* **46** (1993) 239.
19. C-W. Chao, Y-Y. Wang, C-C. Wan and J.T. Yang, *J. Power Sources* **55** (1995) 243.
20. R.H. Newnham and W.G.A. Baldsing, *J. Power Sources* **66** (1997) 27.
21. K.K. Constanti, A.F. Hollenkamp, M.J. Koop and K. McGregor, *J. Power Sources* **55** (1995) 269.
22. H. Dietz, H.K. Niepraschk and K. Wiesener, *J. Power Sources* **46** (1993) 191.
23. V.E. Dmitrenko, B.Z. Lubenstov, S.G. Yevdokimenko, I.I. Lisyansky and V.A. Soldatenko, *J. Power Sources* **67** (1997) 111.
24. A.G. Gad Allah, H.A.A. El-Rahman and M.A. El-Galil, *J. Appl. Electrochem.* **25** (1995) 682.
25. T. Torcheux, J.P. Vaurijoux and A. de Guibert, *J. Power Sources* **64** (1997) 81.
26. R. Wagner, *J. Power Sources* **53** (1995) 153.
27. Y. Yamaguchi, M. Shiota, Y. Nakayama, N. Hirai and S. Hara, *J. Power Sources* **85** (2000) 22.
28. S. Cheng, J. Zhang, M. Zhao and C. Cao, *J. Alloys and Compds* **293-295** (1999) 814.
29. J.P. Diard, B.L. Gorrec and C. Montella, *J. Power Sources* **70** (1998) 78.
30. J.P. Diard, B. Le Gorrec, C. Montella and P. Landaud, *Electrochim. Acta* **42** (1997) 3417.
31. D. Pavlov and G. Petkova, *J. Electrochem. Soc.* **149** (2002) A654.
32. P.R. Roberge, E. Halliop, G. Verville and J. Smit, *J. Power Sources* **32** (1990) 261.
33. S.A.G.R. Karunathilaka, R. Barton, M. Hughes and N.A. Hampson, *J. Appl. Electrochem.* **15** (1985) 251.
34. B.A. Boukamp, 'Equivalent Circuit (Equivcrt.pas) User Manual' (University of Twente, Enschede, The Netherlands, 1989), report CT88/265/128-CT89/214/128.